HHS Public Access

Author manuscript

ACS Appl Mater Interfaces. Author manuscript; available in PMC 2019 October 31.

Published in final edited form as:

ACS Appl Mater Interfaces. 2018 October 31; 10(43): 36786–36795. doi:10.1021/acsami.8b15368.

Nanoparticle-Mediated Acoustic Cavitation Enables High Intensity Focused Ultrasound Ablation Without Tissue Heating

Adem Yildirim[*,†], **Dennis Shi**[†], **Shambojit Roy**[†], **Nicholas T. Blum**[†], **Rajarshi Chattaraj**[‡], **Jennifer N. Cha**[†], **Andrew P. Goodwin**[*,†]

[†]Department of Chemical and Biological Engineering, University of Colorado Boulder. Boulder, Colorado 80303, United States

[‡]Department of Mechanical Engineering, University of Colorado Boulder. Boulder, Colorado 80309, United States

Abstract

While thermal ablation of various solid tumors has been demonstrated using high intensity focused ultrasound (HIFU), the therapeutic outcomes of this technique are still unsatisfactory because of common recurrence of thermally ablated cancers and treatment side effects due to the high ultrasound intensity and acoustic pressure requirements. More precise ablation of tumors can be achieved by generating cavitating bubbles in the tissue using shorter pulses with higher acoustic pressures, which induce mechanical damage rather than thermal. However, it has remained as a challenge to safely deliver the acoustic pressures required for mechanical ablation of solid tumors. Here, we report a method to achieve mechanical ablation at lower acoustic pressures by utilizing phospholipid-stabilized hydrophobic mesoporous silica nanoparticles (PL-hMSN). The PL-hMSNs act as seeds for nucleation of cavitation events and thus significantly reduce the peak negative pressures and spatial-average temporal-average HIFU intensities needed to achieve mechanical ablation. Substantial mechanical damage was observed in the red blood cell or tumor spheroid containing tissue mimicking phantoms at PL-hMSN concentrations as low as 10 μg mL $^{-1}$, after only 5 s of HIFU treatment with peak negative pressures ~11 MPa and duty cycles ~0.01%. Even the application of HIFU (peak negative pressure of 17.5 MPa and duty cycle of 0.017%) for 1 min in the presence of PL-hMSN (200 μg mL^{-1}) did not cause any detectable temperature increase in tissue-mimicking phantoms. In addition, the mechanical effects of cavitation promoted by PL-hMSNs were observed up to 0.5 mm from the center of the cavitation events. This method may thus also improve delivery of therapeutics or nanoparticles to tumor environments with limited macromolecular transport.

Graphical abstract

[*]**Corresponding Author** (Andrew P. Goodwin): andrew.goodwin@colorado.edu. [*](Adem Yildirim): adem.yildirim@colorado.edu.

Author Contributions

The manuscript was written through contributions of all authors. All authors have given approval to the final version of the manuscript.

Supporting Information. A PDF containing a table and additional figures. This material is available free of charge via the Internet at http://pubs.acs.org.

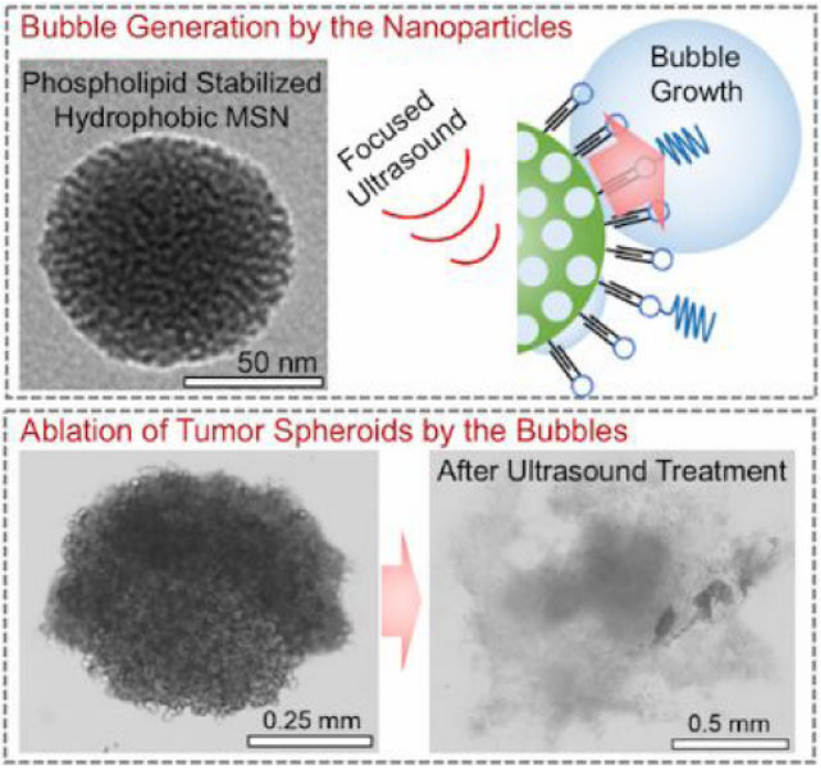

Keywords

High intensity focused ultrasound; tumor ablation; cavitation; mesoporous silica nanoparticles; cancer therapy

INTRODUCTION

Ablation of soft tissue using minimally invasive modalities such as high intensity focused ultrasound (HIFU), lasers, and radiofrequencies are expected to play an increasingly important role in treatment of solid tumors and other localized diseases.[1–7] As alternatives to open surgery, these methods offer better precision, lower cost, decreased morbidity and mortality rates, and shorter recovery times.[8–10] Among these modalities, HIFU is especially promising, owing to the low acoustic attenuation of soft tissue at therapeutic frequencies (~0.5–3.5 MHz), which enables non-invasive ablation of deep tissue.[1] In HIFU ablation, high intensity ultrasound pulses are concentrated into a cigar-shaped focal zone with millimeter orthogonal resolution.[11, 12] At sufficiently high acoustic powers, HIFU can generate a rapid temperature increase (>50 °C) in the tissue and almost immediately cause the formation of necrotic tissue.[1] Leveraging this rapid temperature increase, HIFU has been applied to thermally ablate various benign and malignant tumors and tissues, including uterine fibroids, and tumors in the breast, prostate, kidney, liver, bone, and pancreas.[7, 13–17] However, the therapeutic outcomes of the thermal HIFU ablation of malignant tumors are still unsatisfactory because of common recurrence of the ablated cancers, typically due to

surviving cancer cells peripheral to the treatment area, as well as treatment side effects such as skin burn, damage to the neighboring healthy tissue, and enteroparalysis.[18–20]

These limitations of the efficacy of thermal ablation can be overcome if damage is caused by mechanical effects rather than thermal.[21, 22] Mechanical damage is achieved with shorter, microsecond HIFU pulses with higher peak negative pressures. Rather than depositing thermal energy, this approach produces cavitating bubbles, which are nucleated by the residual gas pockets in the tissue.[23] Cavitation events result in mechanical fractionation of the tissue without causing a significant temperature increase and thus without leaving a necrotic lesion. However, cavitation events are difficult to control at such high acoustic pressures because any gas pocket present in the tissue may act as a nucleation site for initiation of random cavitation events.

Utilization of ultrasound contrast agents (UCAs) can reduce the high peak negative pressures required to induce cavitation (>20 MPa) by acting as nucleation sites for acoustic cavitation.[24, 25] Not only do UCAs reduce the peak negative pressures required for achieving cavitation, but also they can significantly reduce the treatment time needed for complete ablation of large (> 5 cm) tumors, which might take several hours.[1, 20] However, currently existing UCAs, such as stabilized perfluorocarbon microbubbles and nanodroplets, and perfluorocarbon loaded polymer or silica shells, are limited by their large size (usually > 200 nm), which prevents their penetration and accumulation in solid tumors.[26, 27] In addition, encapsulated perfluorocarbons are released rapidly under HIFU insonation due to the rupture of their stabilizing shells, which allows cavitation for only very short time periods, typically less than a minute.[28]

In this study, we report mechanical HIFU treatment by utilizing phospholipid-stabilized hydrophobic mesoporous silica nanoparticles (PL-hMSN), a robust and nanoscale UCAs recently developed by our group.[29] With their smaller sizes (~100 nm) and better storage stability (up to 4 months in PBS with no activity loss[30]) compared to fluid-based contrast agents such as fluorocarbon microbubbles or nanoemulsions, and air-trapped liposomes, these nanoscale UCAs are very promising for tumor imaging and ablation applications. More importantly, unlike fluid-based contrast agents, PL-hMSNs have long-lived activity (for ten minutes) even under extended insonation at cavitation-inducing conditions. As a result, we report a mechanical HIFU treatment approach with spatial-peak pulse-average (I_{sppa}) and spatial-average temporal-average (I_{sata}) intensities of 13,000 and 1.3 W/cm^2, respectively, and treatment durations ~5 s. Cavitation events sensitized by the PL-hMSNs produced mechanical damage in tissue-mimicking agarose phantoms without any detectable temperature increase after treatment. In comparison, spatial-average temporal-average HIFU intensities applied in previous studies were a few orders of magnitude higher than the intensities reported in the present study.[22, 23, 26, 31–34] We first report the excellent acoustic activity and stability of PL-hMSN at concentrations as low as 10 μg mL^{-1} in agarose phantoms. Next, we show mechanical damage induced by the PL-hMSNs under HIFU insonation using red blood cell or tumor spheroid containing agarose phantoms. Finally, we show the propulsion of the nanoscale UCAs into the surrounding hydrogel due to the cavitation events generated by them, which makes the nanoscale UCAs very promising in drug or nanoparticle delivery applications to tumors.

RESULTS AND DISCUSSION

The UCAs used in this study were hydrophobically-modified mesoporous silica nanoparticles, which were stabilized by monolayer of phospholipids and phospholipid-polymer conjugates (Figure 1a).[29] The hydrophobic interface between particles and the phospholipid layers stabilizes air pockets during phospholipid stabilization step. Such air pockets then act as nucleation sites for bubble growth under reduced the acoustic pressures of HIFU (Figure 1b).[28–30, 35–38] The bubbles then grow outside the particle to sizes around 50–200 μm and followed by their violent collapse.[39] The phospholipid stabilized hydrophobic mesoporous silica nanoparticles, PL-hMSNs, were prepared according to our previous report with some modifications.[29] Briefly, mesoporous silica nanoparticles[40–42] were prepared with diameters around 100 nm, and their surfaces were then hydrophobically modified using dodecyl trichlorosilane.[29] Also, fluorescein was incorporated within the silica matrix for fluorescent labeling. Hydrophobically modified particles were then coated with phospholipid layers using 1,2-dipalmitoyl-sn-glycero-3-phosphocholine (DPPC) and 1,2-distearoyl-sn-glycero-3-phospho-ethanolamine-N-[methoxy (polyethylene glycol)-2000] (DSPE-PEG2k) (Figure 1a). PL-hMSN morphology was investigated using Transmission Electron Microscopy (TEM), which found 100 nm nanoparticles filled with ~3 nm sized randomly oriented pores (Figure S4a, b). The phospholipid layers were imaged by negative staining with uranyl acetate, appearing as bright layers (Figure S4c). The presence of the phospholipid layers was further confirmed using Thermogravimetric Analysis (TGA) (Figure S5). Both Nanoparticle Tracking Analysis (NTA) and Dynamic Light Scattering (DLS) methods showed that the PL-hMSN were well-dispersed in PBS (10 mM, pH 7.4) with average particle sizes of 178 nm and 160 nm, respectively (Figure S6).

The acoustic cavitation activity of the PL-hMSN was evaluated using the experimental set-up that was described in our previous reports (Figure S7).[30, 43–45] In a typical experiment, a PL-hMSN dispersion in PBS was placed in the bulb of a plastic pipette, which was in turn directly placed on the coupling cone of a HIFU transducer operating at 1.1 MHz. The generated bubbles under HIFU insonation were detected using a phased array scanning probe (Acuson 4V1) operating at 1.5 MHz in Cadence Contrast Pulse Sequencing (CPS) mode. PL-hMSN samples at different concentrations between 5 and 200 μg mL^{-1} were insonated with 14.1 μs HIFU pulses with a peak negative pressure of 16.8 MPa at a repetition frequency of 10 Hz (duty cycle of 0.014%). To quantify the ultrasound contrast generated by PL-hMSN, three 15 s videos (30 frames per second) were recorded for each sample, and the brightness of the region of interest was quantified using MATLAB (Mathworks, Inc.). Bubble generation was observed at concentrations as low as 5 μg mL^{-1} (Figure S8), which corresponds to 1.9×10^9 particles mL^{-1} according to NTA measurements. In addition, the cavitation events generated by PL-hMSN under HIFU insonation were detected using a passive cavitation detector (PCD) (Figure S9).

As tissue mimicking phantoms, agarose gels were used in this study due to their ease of preparation, transparency, and mechanical properties similar to various solid tumors.[25] First, the acoustic activity of the PL-hMSN was tested in agarose hydrogels. To prepare agarose hydrogels containing PL-hMSN, agarose was first dissolved in PBS by heating to ~90 °C. The solutions were cooled to ~40 °C, and PL-hMSN was added to give final PL-hMSN

concentrations between 0 and 200 μg mL^{-1}. Finally, samples were transferred into the bulbs of plastic pipettes and kept at room temperature (~20 °C) for 1 d to allow the gel to solidify. The acoustic activity of the PL-hMSN in an agarose gel was investigated using the experimental set-up described above. Observable acoustic contrast was detected from the PL-hMSN in the agarose gels at concentrations as low as 10 μg mL^{-1} (Figure 1c). No contrast was detected in the gels in the absence of PL-hMSN. As another control, MSNs without hydrophobic modification were tested in agarose gels at particle concentrations of 200 μg mL^{-1}, but no contrast was detected at the same HIFU conditions. These results confirm that the acoustically active bubbles were only nucleated by PL-hMSN with hydrophobic functionalization.[29, 30, 35] In addition, PL-hMSNs (200 μg mL^{-1}) produced strong ultrasound contrast in agarose gels for ~10 min under continuous HIFU insonation, which demonstrates the substantial stability of these nanoparticle-based UCAs to cavitation (Figure 1d). Finally, we investigated the effects of peak negative pressure and pulse duration on the acoustic activity of the PL-hMSN (200 μg mL^{-1}) encapsulated in agarose gels (Figure S10). PL-hMSN generated acoustically active bubbles in the agarose gels at peak negative pressures and pulse durations as low as 6.4 MPa and 10 μs, respectively.

To evaluate the mechanical damage induced by the PL-hMSN under HIFU insonation, tissue-mimicking multilayer agarose phantoms were prepared.[46] In general, a thin agarose gel layer (~1 mm) containing PL-hMSN and red blood cells (RBCs) or tumor spheroids was sandwiched between two pure agarose gels. The cavitation events were generated in this middle layer and the resulting mechanical damage was observed using RBCs or tumor spheroids as markers. The pure agarose bottom and top layers, with thicknesses of ~2 mm and ~5.5 mm, respectively, were used to support the thin middle layer for easy handling of the phantoms during experiments. In initial studies, RBC phantoms with middle test layers containing RBCs and PL-hMSN (200 μg mL^{-1}) were used (Figure 2a). Figure 2b shows a typical image of an RBC phantom with dimensions of ~3.5 cm in diameter and ~8.5 mm total height. Optical microscopy images of the RBC phantoms (Figure 2c, d) revealed that the RBCs preserved their morphology after encapsulation in agarose gels and were well-dispersed without any agglomeration. For HIFU treatment, RBC phantoms were placed on the coupling cone of the HIFU transducer and ultrasound gel was applied between gels and the transducer to ensure good contact (Figure 2e). Hydrophone measurements showed that the RBC layer of the phantom was in the focal zone of the HIFU transducer when the RBC phantom was directly placed on the coupling cone (see SI for details, Figure S2a). Multiple HIFU treatments were performed for each gel. Figures 2f and g show nine ablated regions in a typical RBC phantom containing PL-hMSN (200 μg mL^{-1}) after HIFU treatment for 30 s at a peak negative pressure of 16.8 MPa, pulse duration of 16.8 μs, and pulse repetition frequency of 10 Hz (duty cycle of 0.017%). The HIFU treated regions appeared less red due to the ablation of RBCs. We also sliced the HIFU-treated RBC phantoms to image the ablated areas in cross-section. Figures 2h and i show the typical image of a sliced phantom, where RBC containing middle layer and three ablated regions are clearly visible. The ablated regions were imaged in more detail using optical microscopy. Figure 2j shows the optical microscope image of an ablated area with a diameter of ~2.7 mm, which was generated by merging four images taken at 5x magnification. The close-up image taken from the center of the ablated section shows the ablation of the RBCs is more pronounced in this

area (Figure 2k). Importantly, very little damage was observed in the absence of PL-hMSN or the presence of MSNs (200 μg mL^{-1}) in the RBC phantoms (Figure S11), indicating that the ablation of RBCs was induced by the mechanical effects sensitized by the PL-hMSNs. Images were then processed using ImageJ (NIH) to assess the ablated areas. In the presence of PL-hMSN, the ablated region is >13x larger than the ablated region observed at other conditions (Figure 2l). Finally, we calculated the ablation area fraction by dividing the ablated area by the area of the whole treated region. While the ablation area fraction exceeds 63% in the presence of PL-hMSN, it was only ~1.5% in the absence of PL-hMSN and ~4.5% in the presence of MSN without hydrophobic modification (Figure 2l).

We also studied the effects of HIFU conditions and PL-hMSN concentration on the size of the ablated lesion and the ablation area fraction. First, particle concentration was varied between 25 and 200 μg mL^{-1} while keeping the HIFU parameters constant (peak negative pressure of 16.8 MPa, pulse duration of 16.8 μs, pulse repetition rate 10 Hz, and treatment duration of 30 s). Significant improvement in the ablation area fraction was observed at particle concentrations as low as 25 μg mL^{-1} (Figure 3a). The ablation area fraction reached a maximum at the particle concentration of around 100 μg mL^{-1}. Next, we investigated the effect of peak negative pressure while keeping the PL-hMSN concentration (200 μg mL^{-1}) and other HIFU parameters constant. At peak negative pressures as low as 4.5 MPa improvement in the size of the ablated region was observed, and it gradually increased with increasing peak negative pressure and reached a maximum around a peak negative pressure of 11.5 MPa (Figure 3b). The effect of pulse duration was also evaluated at the fixed peak negative pressure (16.8 MPa) and PL-hMSN concentration (200 μg mL^{-1}). It was observed that a pulse duration as low as 10.4 μs (duty cycle of 0.01%) was enough to improve the ablation area fraction (Figure 3c). Finally, the effect of HIFU treatment duration was investigated at the peak negative pressure of 16.8 MPa, pulse duration of 16.8 μs, and PL-hMSN concentration of 200 μg mL^{-1} (Figure 3d). An ablation area fraction of around 40% was observed even after only 1 s of treatment (only ~10 pulses), reaching 60% fraction at only 5 s treatment (50 pulses). While significant enhancement was achieved at PL-hMSN concentrations as low as 50 μg mL^{-1}, we used a contrast agent concentration of 200 μg mL^{-1} in the rest of this study to ensure proper mechanical damage after treatment. Similarly, following conditions were selected as optimum and used in the rest of the work unless otherwise specified; pulse duration of 16.8 μs, pulse repetition frequency of 10 Hz (duty cycle of 0.017%), peak negative pressure of 16.8 MPa, and treatment duration of 30 s. Also, at these HIFU conditions I_{sppa} was 13,000 W/cm^2 and I_{sata} (−6 dB spatial average area) was only 1.3 W/cm^2. In comparison, peak negative pressures > 20 MPa, duty cycles in the range of 0.2–10%, average HIFU intensities from 2 to 2000 W/cm^2, and treatment durations of > 1 min have been reported to induce cavitation in both in vitro or ex vivo experiments.[22, 23, 26, 31–34]

To investigate the effect of HIFU treatment on transport of PL-hMSNs from the middle layer to other agarose layers of the RBC phantoms, thin slices of treated regions were imaged under the microscope. Figure 4a shows the cross-sectional bright-field and fluorescence microscope images of the RBC phantoms before and after HIFU treatment. The number of RBCs significantly reduced in the HIFU ablated regions. Fluorescence images reveal that before HIFU treatment the PL-hMSN was uniformly dispersed in the middle agarose layer

and did not diffuse to the surrounding agarose layers. After HIFU treatment, however, they penetrated into the adjacent agarose layers up to a distance of ~500 μm (Figure 4b). Nanoparticles penetrated into the both layers as a result of mechanical forces generated by the acoustic cavitation events. While the nanoparticles penetrated into both layers after HIFU treatment, the penetration depth was greater in the direction of the ultrasound (Figure S12 for more images). This is probably due to the drag of the generated bubbles in the direction of the ultrasound by the acoustic radiation forces. Control experiments were also performed by using a RBC phantom, which contains MSNs (200 μg mL^{-1}) in its middle layer. Due to their limited ability in initiating acoustic cavitation at the acoustic pressures used in this study, MSNs could not penetrate into the adjacent agarose layers after HIFU treatment (Figure S13).

To further evaluate the nanoparticle penetration into neighboring agarose layers under HIFU insonation, we designed a different experiment in which two agarose gels were prepared in the presence and absence of the PL-hMSNs, respectively (Figure 5a). The gel without PL-hMSN was placed on top of the gel with PL-hMSN and the gels were treated with HIFU. After treatment, the gels were separated, and nanoparticle penetration into the PL-hMSN free gel was investigated using fluorescence microscopy (Figure 5a). Several bright fluorescent regions in the treated region were observed after HIFU insonation for 30 s. The size of the whole region was around 3 mm, which is similar to the size of the damaged region in the RBC phantoms (Figure 2j). In the absence of HIFU treatment, no fluorescence was observed in the nanoparticle-free gel, indicating that nanoparticle penetration into the adjacent gel layer was initiated mechanical effects generated by the PL-hMSN under HIFU insonation (Figure S14). In addition, mechanical deformation of the gel surface after HIFU treatment was observed by optical microscopy (Figure S15). Because the deformation and fluorescence patterns match well with each other, the nanoparticles were likely propelled into the adjacent gel layer by bubble cavitation that also mechanically deformed the gel surface. Cross-sectional fluorescence images from the sliced gels were also taken to evaluate nanoparticle penetration depth (Figure 5b and Figure S16). In accordance with the results mentioned above with the RBC phantoms, nanoparticle transport was observed for distances up to 500 μm. Together, these results suggest that nanoparticles are propelled to the surrounding media under HIFU insonation by the mechanical forces generated by the cavitation events.[28, 47] In addition, these results show that acoustic radiation forces were not sufficient to generate damage at the interfaces between gel layers or their surfaces, and the observed damage was due to the mechanical forces generated by PL-hMSN.

To determine if the cavitation and nanoparticle penetration caused damage in the adjacent gel layer, RBC phantoms with an additional middle layer (~1 mm thick) containing RBCs but not PL-hMSNs were prepared. The damage in PL-hMSN free layer induced by the cavitation events in the layer containing PL-hMSN was investigated by taking the cross-sectional optical microscope images of the RBC phantom slices. Significant damage was observed primarily at the regions close to the PL-hMSN containing layer (Figures 6 and S17). Fluorescence images of the same areas show that the damage and the nanoparticle penetration patterns match well with each other (Figures 6 and S17). These results indicate that cavitation events generated by PL-hMSNs can ablate the RBCs in the adjacent layer which are close to the layer containing PL-hMSN (< 500 μm).

The success of the RBC ablation experiments encouraged us to test the PL-hMSN for ablation of tumor spheroids at low acoustic intensities. Spheroids composed of 4T1 murine mammary carcinoma cells were prepared and incubated for 2 days before use.[48, 49] The phantoms containing 4T1 spheroids in their middle layer (spheroid phantoms) were prepared in a similar manner to RBC phantom preparation, for which 3–5 spheroids were mixed with the agarose gel solution at 37 °C in PBS and cast as the middle layer in the phantoms (Figure 7a). For these experiments PL-hMSN were prepared without fluorescein labeling (Figure S18) to avoid interference with viability assays. Figure 7b shows a typical image of an encapsulated spheroid in the phantom with a diameter of around 500 μm. After HIFU treatment in the presence of PL-hMSN (200 μg mL^{-1}), the spheroid was almost entirely destroyed by the mechanical effects due to the acoustic cavitation generated in the phantoms (Figure 7c and Figure S19). In the absence of PL-hMSN or the presence of MSNs (200 μg mL^{-1}), spheroids remained mostly intact after HIFU treatment (Figure 7d and Figure S19). It should be noted that spheroid destruction induced by the PL-hMSNs encapsulated in the gel surrounding them. Thus, PL-hMSNs do not necessarily have to penetrate into the spheroids to ablate them because of the long-range mechanical effects observed up to 0.5 mm away from the ablation site.

The viability of the 4T1 spheroids before and after HIFU treatment were evaluated by addition of calcein AM reagent. The bright calcein AM fluorescence was observed for the untreated spheroids (Figure 7d), suggesting that the cells in the spheroids mostly remain viable after encapsulation in phantoms. Figure 7c shows a typical image of HIFU treated spheroids in the presence of PL-hMSNs (Figure S16), where only a weak residual fluorescence was observed. The residual fluorescence may be due to the released intracellular esterases from the ablated cells, which converts the calcein AM to the fluorescent calcein by the hydrolysis of acetoxymethyl group.[50] In the absence of PL-hMSN or the presence of regular MSN, there was no noticeable decrease in the calcein AM fluorescence (Figure 7d and Figure S19) indicating that the spatial-average temporal-average HIFU intensities used in this study did not significantly decrease the viability of the cells in the absence of PL-hMSN. Also, as a positive control, spheroid phantoms containing dead spheroids were prepared by keeping the spheroids at 75 °C for 15 min; no fluorescence was detected in these after staining (Figure 7d). Figure 7e shows the average fluorescence intensity of each of the spheroid experiments. After HIFU treatment in the presence of PL-hMSN, a decrease of around 85% was observed in the fluorescence intensity, while other conditions showed no statistically significant decrease in the fluorescence intensities. Finally, one of the main hypotheses of this work is that the HIFU effects sensitized by the PL-hMSNs are purely mechanical rather than thermal because the HIFU doses used in this study were up to three orders of magnitude lower than the HIFU doses used in literature. In fact, we did not observe any detectable temperature increase by measuring the temperature of the agarose gel phantoms before and after HIFU treatment for 1 min using a thermocouple (Figure S20). Thus, the cell death observed for these spheroids was induced by mechanical means rather than by thermal effects.

CONCLUSIONS

In summary, a method for ultrasound ablation was demonstrated using phospholipid stabilized hydrophobic mesoporous silica nanoparticles that could sensitize the spatial-average temporalaverage HIFU intensities up to three orders of magnitude smaller than that needed for conventional thermal HIFU treatment. The nanoparticles acted as artificial seeds for nucleation to significantly reduce the acoustic pressures needed to generate acoustic cavitation in tissue-mimicking phantoms. The ablation of the cells by the mechanical effects created by these novel UCAs was demonstrated by first using RBCs and then tumor spheroids encapsulated in the phantoms. Importantly, these mechanical impacts were observed up to relatively long distances (0.5 mm) from the center of the cavitation events. While the validation of acoustic cavitation generation by the PL-hMSN in vivo is beyond of the scope of this study, the literature suggests that acoustic cavitation events can be generated by UCAs in solid tumors.[28, 51, 52] Therefore, we believe that with their small size, exceptional stability, and high acoustic activity, the PL-hMSN have considerable potential in ablation of solid tumors at safe HIFU intensities, and future studies will explore this possibility. In addition, the relatively long-range “blast radius” can be applied to improve the efficacy of drug, gene, or nanoparticle delivery to tumors with limited transport.

MATERIALS AND METHODS

Materials.

Tetraethylorthosilicate (TEOS) was purchased from Acros Organics. Cetyltrimethylammonium chloride solution (CTAC, 25% in water), trichlorododecylsilane, and Poly(2-hydroxyethyl methacrylate) were purchased from Sigma Aldrich. Chloroform and hexanes were purchased from Merck. Agarose type II (low gelling temperature) was ordered from Amresco, Inc. EDTA stabilized whole bovine blood was ordered from Lampire Biological Laboratories. Ethanol was purchased from Decon Labs. 1,2-dipalmitoyl-sn-glycero-3-phosphocholine (DPPC) and 1,2-distearoyl-sn-glycero-3-phospho-ethanolamine-N-[methoxy (polyethylene glycol)-2000] (DSPE-PEG2k) were ordered from Avanti Polar Lipids. The 4T1 cell line was purchased from American Type Culture Collection. Calcein AM was purchased from Invitrogen (Thermo Fisher Scientific).

Synthesis of MSNs and hMSNs.

Fluorescein-labeled MSNs and hydrophobically modified MSNs (hMSN) were previously synthesized[29] and stored at ambient conditions. For spheroid ablation experiments unlabeled MSNs were prepared in the absence of fluorescence labeling and hydrophobically modified as described in our previous report.[29]

Preparation of PL-hMSNs.

To stabilize hMSN with phospholipid coatings, 4 mg of hMSN was dispersed in 1 mL of chloroform with brief sonication, and 0.5 mL of DPPC (4 mg mL^{-1}, in chloroform) and 0.3 mL of DSPE-PEG2k (2 mg mL^{-1}, in chloroform) solutions were added to the nanoparticle dispersion. Chloroform was evaporated at 75 °C by keeping in a water bath for 1 h. Dried nanoparticles and phospholipids were suspended in 2 mL of deionized water and bath

sonicated for 3 min. The suspended nanoparticles were stirred at 75 °C for 45 min. Finally, they were precipitated by centrifugation (10,000 rcf) and washed with deionized water.

PL-hMSN characterization.

Transmission electron microscopy (TEM) images of the nanoparticles were taken using a T12 Spirit (FEI Tecnai) microscope. To stain the phospholipid layers around the nanoparticles, 2% uranyl acetate solution was applied on carbon-coated TEM copper grids. Thermal gravimetric analyses (TGA) of the nanoparticles were performed using a TGA/DSC 1 Star System (Mettler Toledo) under nitrogen atmosphere. Dynamic Light Scattering (DLS) analysis of the PL-hMSN dispersed in phosphate buffered saline (PBS, pH 7.4, 10 mM) was performed using a Litesizer 500 (Anton Paar). Nanoparticle Tracking Analysis (NTA) of the PL-hMSN dispersed in phosphate buffered saline (PBS, pH 7.4, 10 mM) was performed using a NanoSight LM10 setup (Malvern).

Ultrasound imaging set up.

Ultrasound contrast generation experiments by the nanoparticles and HIFU treatment of agarose gels were performed according to our previous reports.[29, 30, 35, 43–45] For HIFU exposure, a spherically focused, single-element, HIFU transducer (Sonic Concepts H101, 64.0 mm Active Diameter by 63.2 mm Radius of Curvature) equipped with a coupling cone (Sonic Concepts C101) was used. The HIFU transducer was connected to a 30 MHz Function/Arbitrary Waveform Generator (Agilent Technologies) via an AG Series Amplifier (T&C Power Conversion, Inc.), the amplifier operating at 100% output (Figure S7). A capsule hydrophone (HGL-0400, Onda Corp.) was used to estimate the peak negative and peak positive pressures, pulse duration, and focal dimensions of the HIFU pulses (See SI for details, Figure S1, and Table S1). The following HIFU parameters were used: 1.1 MHz center frequency, peak negative pressures between 4.5 and 17.5 MPa, pulse repetition frequency of 10 Hz, and pulse durations between 9.5 and 19.5 μs (duty cycles between 0.01% and 0.02%).

To investigate bubble generation by the nanoparticles, nanoparticles were dispersed in 1 mL of Phosphate Buffered Saline (PBS, 10 mM, pH 7.4) and placed within the bulb of a plastic pipette with the stem pointed upwards. The plastic bulb containing the sample was positioned on top of the coupling cone of the HIFU transducer, which was submerged in a water tank. To image the generated bubbles under HIFU insonation, a Siemens Acuson Sequoia C512 scanner was used. A vector array 4V1 (Acuson) transducer (1–4 MHz) was orthogonally aligned to acquire horizontal cross-sectional images and videos (15 s-10 min) of the samples. The transducer was connected to the scanner operating in cadence pulse sequencing (CPS) mode at 1.5 MHz and a mechanical index (MI) of 0.19. The brightness in the region of interest of each video frame was calculated using a MATLAB (Mathworks, Inc.) code.

To test the bubble generation by nanoparticles in agarose gels, first, 1.2 % (w/v) agarose solution in PBS was prepared by dissolving the agarose at ~ 90 °C. Then the agarose solution was cooled down to 40 °C and 0.83 of mL of the agarose solution was mixed with 0.17 of mL PBS containing nanoparticles at different concentrations (final particle

concentrations between 0 and 200 μg mL^{-1} and final agarose concentration is 1%) and transferred in the bulbs of the plastic pipettes. The agarose phantoms were kept at room temperature (20 °C) overnight for complete solidification. The generated bubbles under HIFU treatment were imaged as described above.

PCD measurements.

For PCD measurements, a 20 MHz single element immersion transducer (Olympus Corp.) was used. This was connected to a 5072PR Pulser/Receiver (Olympus Corp.) operating with +40dB gain in receive-only mode. A EF513 6.7 MHz high pass filter (ThorLabs, Inc.) was used to eliminate any contributions from the HIFU and it connected between output of the Pulser/Receiver and a Tektronix TDS2012C oscilloscope. The external trigger of the oscilloscope was connected to a Function/Arbitrary Waveform Generator (Agilent Technologies) so that each waveform triggers an oscilloscope reading.

Purification of Red Blood Cells (RBCs).

RBCs were purified from bovine whole blood as described elsewhere.[53] Briefly, 2 mL of whole blood were centrifuged at 300 rcf for 5 min to remove blood plasma and the surface layer. Then, RBCs were redispersed in 5 mL of PBS (pH 7.4, 10 mM) by gentle shaking, centrifuged again at 300 rcf for 5 min, and the supernatant was discarded. This washing step was repeated three times, and RBCs were dispersed in 2 mL PBS and used immediately after preparation.

Preparation of RBC phantoms.

Multi-layer phantoms with RBC containing middle layers were prepared according to a previous report.[46] First, 1% (w/v) agarose was dissolved in PBS by heating around 90 °C until a clear solution was obtained. Then, agarose solution was cooled to 40 °C, and 2.25 mL of this solution was poured in a 6-well plate to prepare the bottom layer. This layer was allowed to solidify at RT for 30 min. To prepare middle layer(s), 1.2% (w/v) agarose solution in PBS was prepared as described above and cooled to 37 °C. 1 mL of agarose solution was mixed with 0.1 mL of RBC dispersion in PBS and 0.1 mL of PBS containing or not containing nanoparticles at 37 °C. This mixture was poured onto the first agarose layer and allowed to solidify at RT for 30 min. Finally, 5 mL of 1% (w/v) agarose solution in PBS was used to prepare top layer. The RBC phantoms were kept at RT overnight for further solidification.

Cell culture.

4T1 murine mammary carcinoma cells were grown to confluence at 37 °C under 5 % CO_2 in Roswell Park Memorial Institute (RPMI) 1640 medium supplemented with 10 % fetal bovine serum (FBS), 1% penicillin/streptomycin, and 2 mM L-glutamine.

Preparation of 4T1 spheroids.

4T1 spheroids were prepared according to a previous report in poly(HEMA) coated round-bottom 96-well plates.[48, 49] Poly(HEMA) coated plates were sterilized under UV light for 45

min and 5,000 4T1 cells in 200 μL RPMI-1640 medium (10% FBS) was added to the wells. Plates were incubated at 37 °C under 5 % CO_2 for 2 days to allow spheroid formation.

Preparation of 4T1 spheroid phantoms.

Spheroid phantoms were prepared in 6-well plates. Top and bottom supporting agarose layers were prepared as described above. To prepare the spheroid-containing middle layer, 4–5 spheroids were washed with PBS once and dispersed in 0.1 mL PBS. The spheroids were then mixed with 1 mL of 1.2% (w/v) agarose solution in PBS and 0.1 mL of PBS either containing or not containing nanoparticles (200 μg mL^{-1}) at 37 °C. The gels were allowed to solidify at RT for 1.5 h.

HIFU treatment of the phantoms.

To expose the RBC or spheroid phantoms to HIFU, phantoms were placed onto the coupling cone of the HIFU and treated with HIFU using the parameters mentioned above. An ultrasound transmitting gel (Aquasonic 100, Parker) was applied between the HIFU cone and the phantom to ensure good contact between them. The following HIFU parameters were used: 1.1 MHz center frequency, peak negative pressures between 4.5 and 17.5 MPa, pulse repetition frequency of 10 Hz, and pulse durations between 9.5 and 19.5 μs (duty cycles between 0.01% and 0.02%). After HIFU treatment, the mechanical damage in the phantoms and the penetration of fluorescent nanoparticles were imaged using a Carl Zeiss Ax10 microscope.

Calcein AM staining of HIFU treated agarose phantoms.

For Calcein AM staining, the bottom layers of the three-layered phantoms were removed and 10 μL of 10 μM Calcein AM solution (in PBS) was added onto the spheroids. The spheroids were incubated at RT in the dark for 8 h and imaged using a fluorescence microscope. The total fluorescence intensity of the spheroids was determined using the Image J software.

Supplementary Material

Refer to Web version on PubMed Central for supplementary material.

ACKNOWLEDGMENT

The authors thank Prof. Stephanie J. Bryant for use of her cell culture equipment, Prof. Douglas L. Gin and Richard D. Noble for use of their Mettler Toledo TGA/DSC 1 Star System, and Prof. Mark A. Borden for use of his Onda HNC-0200 needle hydrophone.

Funding Sources

This work was supported by NIH Grant Nos. DP2EB020401 and R03EB021432.

REFERENCES

1. Kennedy JE, High-intensity focused ultrasound in the treatment of solid tumours. Nat. Rev. Cancer 2005, 5 (4), 321–327. [PubMed: 15776004]
2. Lal S; Clare SE; Halas NJ, Nanoshell-Enabled Photothermal Cancer Therapy: Impending Clinical Impact. Acc. Chem. Res. 2008, 41 (12), 1842–1851. [PubMed: 19053240]

3. Chu KF; Dupuy DE, Thermal ablation of tumours: biological mechanisms and advances in therapy. Nat. Rev. Cancer 2014, 14 (3), 199–208. [PubMed: 24561446]
4. Lee N; Yoo D; Ling D; Cho MH; Hyeon T; Cheon J, Iron Oxide Based Nanoparticles for Multimodal Imaging and Magnetoresponsive Therapy. Chem. Rev. 2015, 115 (19), 10637–10689. [PubMed: 26250431]
5. Leinenga G; Goetz J, Scanning ultrasound removes amyloid-beta and restores memory in an Alzheimer's disease mouse model. Sci. Transl. Med. 2015, 7 (278), 278ra33.
6. Manthe RL; Foy SP; Krishnamurthy N; Sharma B; Labhasetwar V, Tumor Ablation and Nanotechnology. Mol. Pharm. 2010, 7 (6), 1880–1898. [PubMed: 20866097]
7. Al-Bataineh O; Jenne J; Huber P, Clinical and future applications of high intensity focused ultrasound in cancer. Cancer Treat. Rev. 2012, 38 (5), 346–353. [PubMed: 21924838]
8. Jolesz FA, MRI-Guided Focused Ultrasound Surgery. Annu. Rev. Med. 2009, 60, 417–430. [PubMed: 19630579]
9. Liu TZ; Zhang N; Wang ZG; Wu MY; Chen Y; Ma M; Chen HR; Shi JL, Endogenous Catalytic Generation of O2 Bubbles for In Situ Ultrasound-Guided High Intensity Focused Ultrasound Ablation. ACS Nano 2017, 11 (9), 9093–9102. [PubMed: 28796487]
10. Goldberg SN; Grassi CJ; Cardella JF; Charboneau JW; Dodd GD; Dupuy DE; Gervais D; Gillams AR; Kane RA; Lee FT; Livraghi T; McGahan J; Phillips DA; Rhim H; Silverman SG, Image-Guided Tumor Ablation: Standardization of terminology and reporting criteria. Radiology 2005, 235 (3), 728–739. [PubMed: 15845798]
11. Kennedy JE; ter Haar GR; Cranston D, High intensity focused ultrasound: surgery of the future? Br. J. Radiol. 2003, 76 (909), 590–599. [PubMed: 14500272]
12. Ter Haar G; Coussios C, High intensity focused ultrasound: Physical principles and devices. Int. J. Hyperth. 2007, 23 (2), 89–104.
13. Zhang L; Chen WZ; Liu YJ; Hu X; Zhou K; Chen L; Peng S; Zhu H; Zou HL; Bai J; Wang ZB, Feasibility of magnetic resonance imaging-guided high intensity focused ultrasound therapy for ablating uterine fibroids in patients with bowel lies anterior to uterus. Eur. J. Radiol. 2010, 73 (2), 396–403. [PubMed: 19108974]
14. Maloney E; Hwang JH, Emerging HIFU applications in cancer therapy. Int. J. Hyperth. 2015, 31 (3), 302–309.
15. Hwang JH; Wang YN; Warren C; Upton MP; Starr F; Zhou YF; Mitchell SB, Preclinical in vivo evaluation of an extracorporeal hifu device for ablation of pancreatic tumors. Ultrasound Med. Biol. 2009, 35 (6), 967–975. [PubMed: 19201519]
16. Wu F; Wang ZB; Cao YD; Chen WZ; Bai J; Zou JZ; Zhu H, A randomised clinical trial of high-intensity focused ultrasound ablation for the treatment of patients with localised breast cancer. Br. J. Cancer 2003, 89 (12), 2227–2233. [PubMed: 14676799]
17. Illing RO; Kennedy JE; Wu F; ter Haar GR; Protheroe AS; Friend PJ; Gleeson FV; Cranston DW; Phillips RR; Middleton MR, The safety and feasibility of extracorporeal high-intensity focused ultrasound (HIFU) for the treatment of liver and kidney tumours in a Western population. Br. J. Cancer 2005, 93 (8), 890–895. [PubMed: 16189519]
18. Hijnen N; Kneepkens E; de Smet M; Langereis S; Heijman E; Grull H, Thermal combination therapies for local drug delivery by magnetic resonance-guided high-intensity focused ultrasound. Proc. Natl. Acad. Sci. U.S.A 2017, 114 (24), E4802–E4811. [PubMed: 28566498]
19. Devarakonda SB; Myers MR; Lanier M; Dumoulin C; Banerjee RK, Assessment of Gold Nanoparticle-Mediated-Enhanced Hyperthermia Using MR-Guided High-Intensity Focused Ultrasound Ablation Procedure. Nano Letters 2017, 17 (4), 2532–2538. [PubMed: 28287747]
20. Liberman A; Wu Z; Barback CV; Viveros RD; Wang J; Ellies LG; Mattrey RF; Trogler WC; Kummel AC; Blair SL, Hollow iron-silica nanoshells for enhanced high intensity focused ultrasound. J. Surg. Res. 2014, 190 (2), 391–398. [PubMed: 24972734]
21. Khokhlova TD; Wang YN; Simon JC; Cunitz BW; Starr F; Paun M; Crum LA; Bailey MR; Khokhlova VA, Ultrasound-guided tissue fractionation by high intensity focused ultrasound in an in vivo porcine liver model. Proc. Natl. Acad. Sci. U.S.A 2014, 111 (22), 8161–8166. [PubMed: 24843132]

22. Parsons JE; Cain CA; Abrams GD; Fowlkes JB, Pulsed cavitational ultrasound therapy for controlled tissue homogenization. Ultrasound Med. Biol. 2006, 32 (1), 115–129. [PubMed: 16364803]

23. Parsons JE; Cain CA; Fowlkes JB, Spatial variability in acoustic backscatter as an indicator of tissue homogenate production in pulsed cavitational ultrasound therapy. IEEE Trans. Ultrason., Ferroelect., Freq. Control 2007, 54 (3), 576–590.

24. Kang ST; Lin YC; Yeh CK, Mechanical bioeffects of acoustic droplet vaporization in vessel-mimicking phantoms. Ultrason. Sonochem. 2014, 21 (5), 1866–1874. [PubMed: 24690297]

25. Vlaisavljevich E; Durmaz YY; Maxwell A; ElSayed M; Xu Z, Nanodroplet-Mediated Histotripsy for Image-guided Targeted Ultrasound Cell Ablation. Theranostics 2013, 3 (11), 851–864. [PubMed: 24312155]

26. Zhou Y; Wang ZG; Chen Y; Shen HX; Luo ZC; Li A; Wang Q; Ran HT; Li P; Song WX; Yang Z; Chen HR; Wang ZB; Lu GM; Zheng YY, Microbubbles from Gas-Generating Perfluorohexane Nanoemulsions for Targeted Temperature-Sensitive Ultrasonography and Synergistic HIFU Ablation of Tumors. Adv. Mater. 2013, 25 (30), 4123–4130. [PubMed: 23788403]

27. Garg S; Thomas AA; Borden MA, The effect of lipid monolayer in-plane rigidity on in vivo microbubble circulation persistence. Biomaterials 2013, 34 (28), 6862–6870. [PubMed: 23787108]

28. Kwan JJ; Myers R; Coviello CM; Graham SM; Shah AR; Stride E; Carlisle RC; Coussios CC, Ultrasound-Propelled Nanocups for Drug Delivery. Small 2015, 11 (39), 5305–5314. [PubMed: 26296985]

29. Yildirim A; Chattaraj R; Blum NT; Shi D; Kumar K; Goodwin AP, Phospholipid Capped Mesoporous Nanoparticles for Targeted High Intensity Focused Ultrasound Ablation. Adv. Healthcare Mater. 2017, 6 (18), 1700514.

30. Xu Z; Raghavan M; Hall TL; Chang CW; Mycek MA; Fowlkes JB; Cain CA, High speed imaging of bubble clouds generated in pulsed ultrasound cavitational therapy-histotripsy. IEEE Trans. Ultrason., Ferroelect., Freq. Control 2007, 54 (10), 2091–2101.

31. Kieran K; Hall TL; Parsons JE; Wolf JS; Fowlkes JB; Cain CA; Roberts WW, Refining histotripsy: Defining the parameter space for the creation of nonthermal lesions with high intensity, pulsed focused ultrasound of the in vitro kidney. J. Urol. 2007, 178 (2), 672–676. [PubMed: 17574617]

32. Xu Z; Fowlkes JB; Rothman ED; Levin AM; Cain CA, Controlled ultrasound tissue erosion: The role of dynamic interaction between insonation and microbubble activity. J. Acoust. Soc. Am. 2005, 117 (1), 424–435. [PubMed: 15704435]

33. Vlaisavljevich E; Kim Y; Allen S; Owens G; Pelletier S; Cain C; Ives K; Xu Z, Image-guided non-invasive ultrasound liver ablation using histotripsy: feasibility study in an in vivo porcine model. Ultrasound Med. Biol. 2013, 39 (8), 1398–1409. [PubMed: 23683406]

34. Yildirim A; Chattaraj R; Blum NT; Goldscheitter GM; Goodwin AP, Stable Encapsulation of Air in Mesoporous Silica Nanoparticles: Fluorocarbon-Free Nanoscale Ultrasound Contrast Agents. Adv. Healthcare Mater. 2016, 5 (11), 1290–1298.

35. Yildirim A; Chattaraj R; Blum NT; Goodwin AP, Understanding Acoustic Cavitation Initiation by Porous Nanoparticles: Toward Nanoscale Agents for Ultrasound Imaging and Therapy. Chem. Mater. 2016, 28 (16), 5962–5972. [PubMed: 28484307]

36. Zhao Y; Zhu Y; Fu J; Wang L, Effective Cancer Cell Killing by Hydrophobic Nanovoid-Enhanced Cavitation under Safe Low-Energy Ultrasound. Chem. Asian J. 2014, 9 (3), 790–796. [PubMed: 24339016]

37. Zhang L; Belova V; Wang HQ; Dong WF; Mohwald H, Controlled Cavitation at Nano/Microparticle Surfaces. Chem. Mater. 2014, 26 (7), 2244–2248.

38. Jin QF; Kang ST; Chang YC; Zheng HR; Yeh CK, Inertial cavitation initiated by polytetrafluoroethylene nanoparticles under pulsed ultrasound stimulation. Ultrason. Sonochem. 2016, 32, 1–7. [PubMed: 27150739]

39. Kwan JJ; Lajoinie G; de Jong N; Stride E; Versluis M; Coussios CC, Ultrahigh-Speed Dynamics of Micrometer-Scale Inertial Cavitation from Nanoparticles. Phys. Rev. Appl. 2016, 6 (4), 044004, 1–8.

40. Dobay MP; Schmidt A; Mendoza E; Bein T; Radler JO, Cell Type Determines the Light-Induced Endosomal Escape Kinetics of Multifunctional Mesoporous Silica Nanoparticles. Nano Letters 2013, 13 (3), 1047–1052. [PubMed: 23406469]
41. Moller K; Kobler J; Bein T, Colloidal suspensions of nanometer-sized mesoporous silica. Adv. Funct. Mater. 2007, 17 (4), 605–612.
42. Liong M; Lu J; Kovochich M; Xia T; Ruehm SG; Nel AE; Tamanoi F; Zink JI, Multifunctional inorganic nanoparticles for imaging, targeting, and drug delivery. ACS Nano 2008, 2 (5), 889–896. [PubMed: 19206485]
43. Blum NT; Yildirim A; Chattaraj R; Goodwin AP, Nanoparticles Formed by Acoustic Destruction of Microbubbles and Their Utilization for Imaging and Effects on Therapy by High Intensity Focused Ultrasound. Theranostics 2017, 7 (3), 694–702. [PubMed: 28255360]
44. Chattaraj R; Goldscheitter GM; Yildirim A; Goodwin AP, Phase behavior of mixed lipid monolayers on perfluorocarbon nanoemulsions and its effect on acoustic contrast. RSC Adv. 2016, 6 (112), 111318–111325.
45. Chattaraj R; Mohan P; Besmer JD; Goodwin AP, Selective Vaporization of Superheated Nanodroplets for Rapid, Sensitive, Acoustic Biosensing. Adv. Healthcare Mater. 2015, 4 (12), 1790–1795.
46. Maxwell AD; Wang TY; Yuan LQ; Duryea AP; Xu Z; Cain CA, A tissue phantom for visualization and measurement of ultrasound-induced cavitation damage. Ultrasound Med. Biol. 2010, 36 (12), 2132–2143. [PubMed: 21030142]
47. Soto F; Mishra RK; Chrostowski R; Martin A; Wang J, Epidermal Tattoo Patch for Ultrasound-Based Transdermal Microballistic Delivery. Adv. Mater. Techol. 2017, 2 (12), 1700210.
48. Steadman K; Stein WD; Litman T; Yang SX; Abu-Asab M; Dutcher SK; Bates S, PolyHEMA spheroids are an inadequate model for the drug resistance of the intractable solid tumors. Cell Cycle 2008, 7 (6), 818–829. [PubMed: 18239467]
49. Ivascu A; Kubbies M, Rapid generation of single-tumor spheroids for high-throughput cell function and toxicity analysis. J. Biomol. Screen. 2006, 11 (8), 922–932. [PubMed: 16973921]
50. Monette R; Small DL; Mealing G; Morley P, A fluorescence confocal assay to assess neuronal viability in brain slices. Brain Res. Protoc. 1998, 2 (2), 99–108.
51. Myers R; Coviello C; Erbs P; Foloppe J; Rowe C; Kwan J; Crake C; Finn S; Jackson E; Balloul JM; Story C; Coussios C; Carlisle R, Polymeric Cups for Cavitation-mediated Delivery of Oncolytic Vaccinia Virus. Mol. Ther. 2016, 24 (9), 1627–1633. [PubMed: 27375160]
52. Ashida R; Kawabata K; Maruoka T; Asami R; Yoshikawa H; Takakura R; Ioka T; Katayama K; Tanaka S, New approach for local cancer treatment using pulsed high-intensity focused ultrasound and phase-change nanodroplets. J. Med. Ultrason. 2015, 42 (4), 457–466.
53. Lin YS; Haynes CL, Impacts of Mesoporous Silica Nanoparticle Size, Pore Ordering, and Pore Integrity on Hemolytic Activity. J. Am. Chem. Soc. 2010, 132 (13), 4834–4842. [PubMed: 20230032]

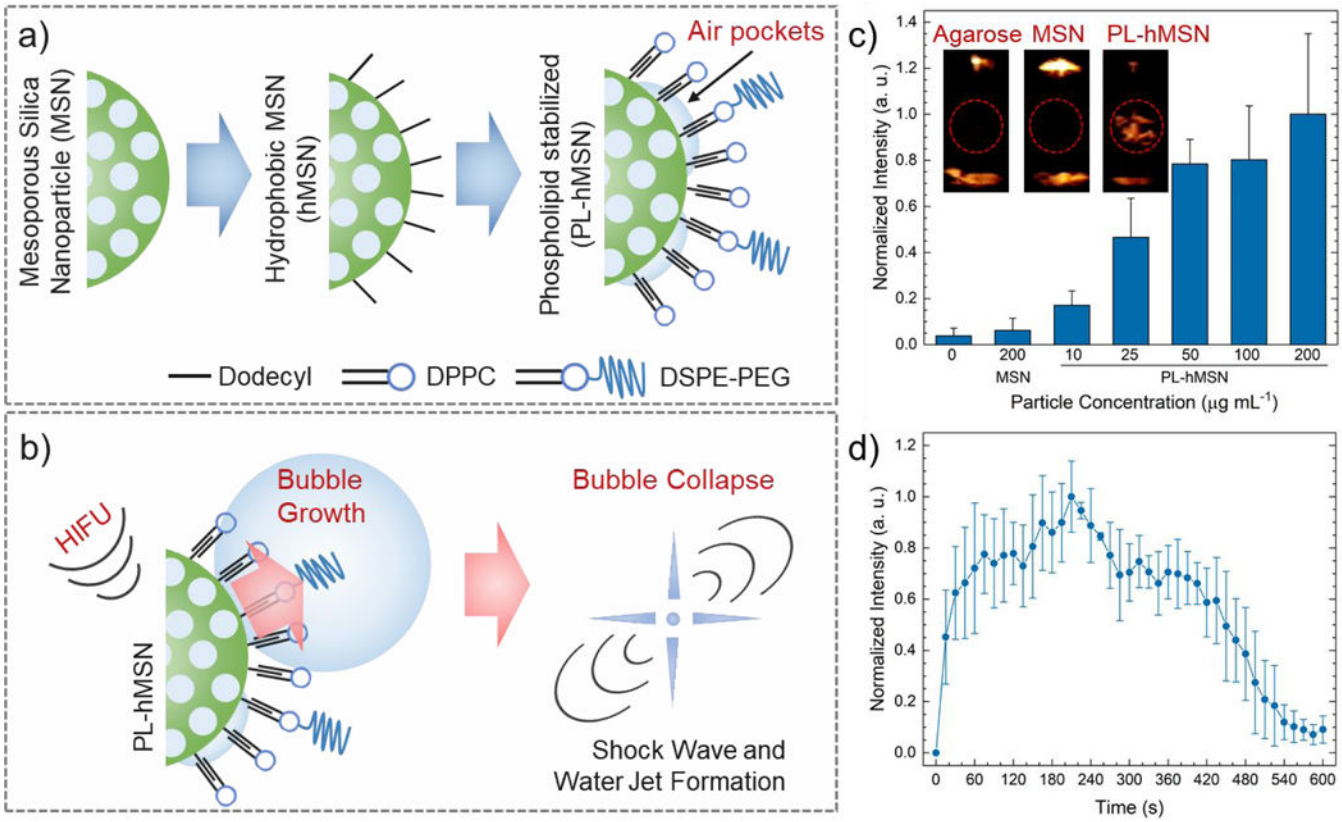

Figure 1.

a) Schematic representation of ultrasound contrast agent preparation. b) Schematic of acoustic cavitation initiation by the PL-hMSN under HIFU insonation. c) Normalized ultrasound contrast intensities calculated from the acquired movies of agarose samples containing MSN or PL-hMSN at different concentrations, which were exposed to HIFU for 15 s at a pulse duration of 16.8 μs, a pulse repetition frequency of 10 Hz (duty cycle of 0.017%), and a peak negative pressure of 16.8 MPa. Insets are the representative images taken from movies acquired during HIFU irradiation in the presence or absence of nanoparticles (200 μg mL^{-1}). Red circles indicate the region of interest in the images. d) Normalized ultrasound contrast intensity calculated from the three acquired movies of agarose samples containing PL-hMSN at 200 μg mL^{-1}, which were exposed to HIFU for 10 min at a pulse duration of 16.8 μs, a pulse repetition frequency of 10 Hz (duty cycle of 0.017%), and peak negative pressure of 16.8 MPa. Error bars = 1 SD, studies were run in triplicate.

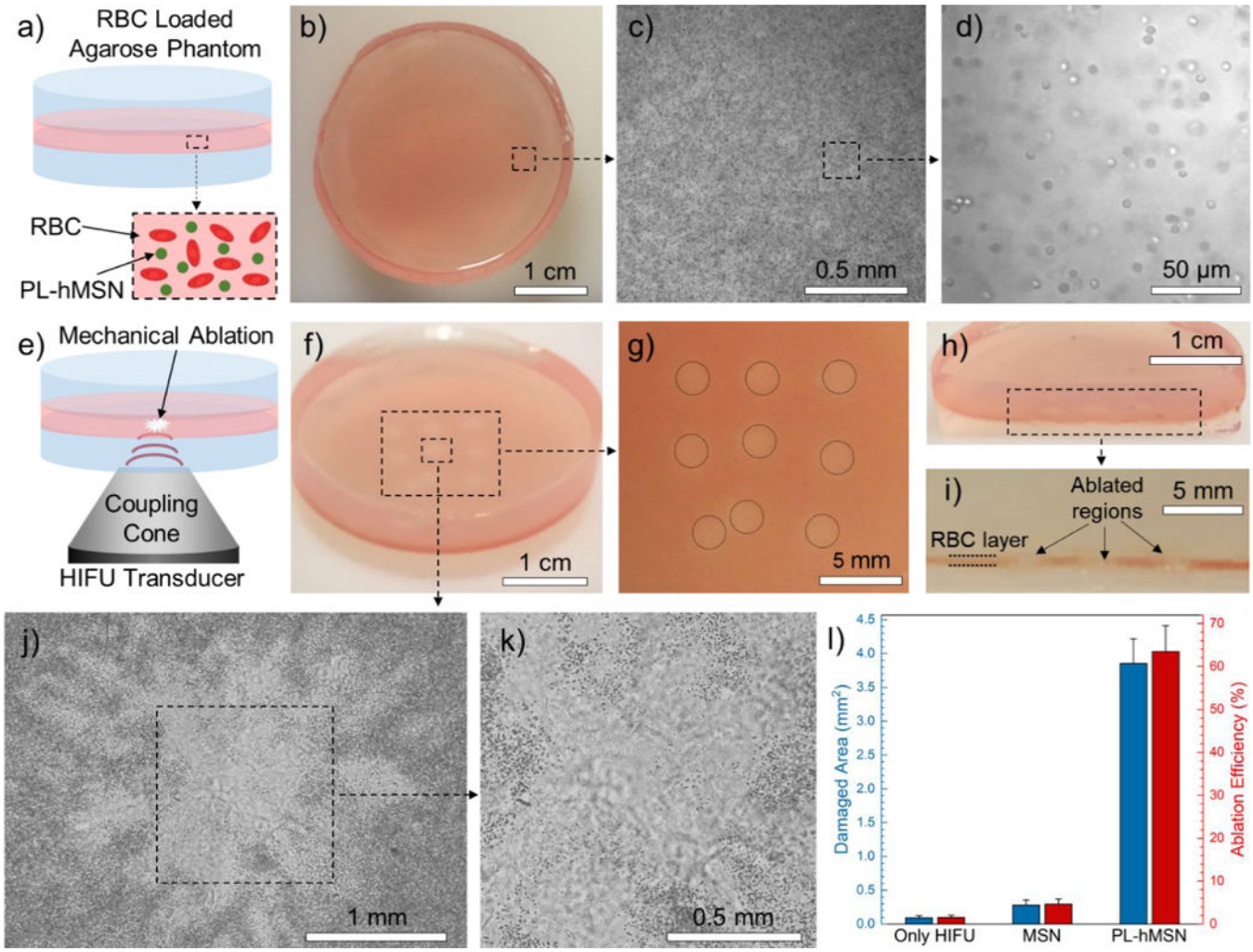

Figure 2.

a) Schematic showing the RBC phantoms. b) Photograph showing a RBC phantom. c) 5x optical microscope image of the RBCs encapsulated in agarose phantoms. d) Close-up optical microscope image of the RBC phantom taken at 40x magnification showing that the encapsulated RBCs showed preserved morphology. e) Schematic representation of the HIFU treatment of the RBC phantoms. f) Photograph of a HIFU treated RBC phantom containing PL-hMSN (200 μg mL^{-1}) for 30 s at a pulse duration of 16.8 μs, a pulse repetition frequency of 10 Hz (duty cycle of 0.017%), and peak negative pressure of 16.8 MPa. g) Close-up image of the RBC phantom in (f) showing the nine ablated regions. h) and i) Photographs of a sliced RBC phantom containing PL-hMSN (200 μg mL^{-1}) after HIFU treatment showing the cross-sectional appearance of three ablated regions. j) and k) Optical microscope images of an ablated region. l) Damaged areas and ablation area fractions in the RBC phantoms containing or not containing nanoparticles (200 μg mL^{-1}) after HIFU treatment for 30 s at a pulse duration of 16.8 μs and peak negative pressure of 16.8 MPa. Error bars = 1 SD, studies were run in triplicate.

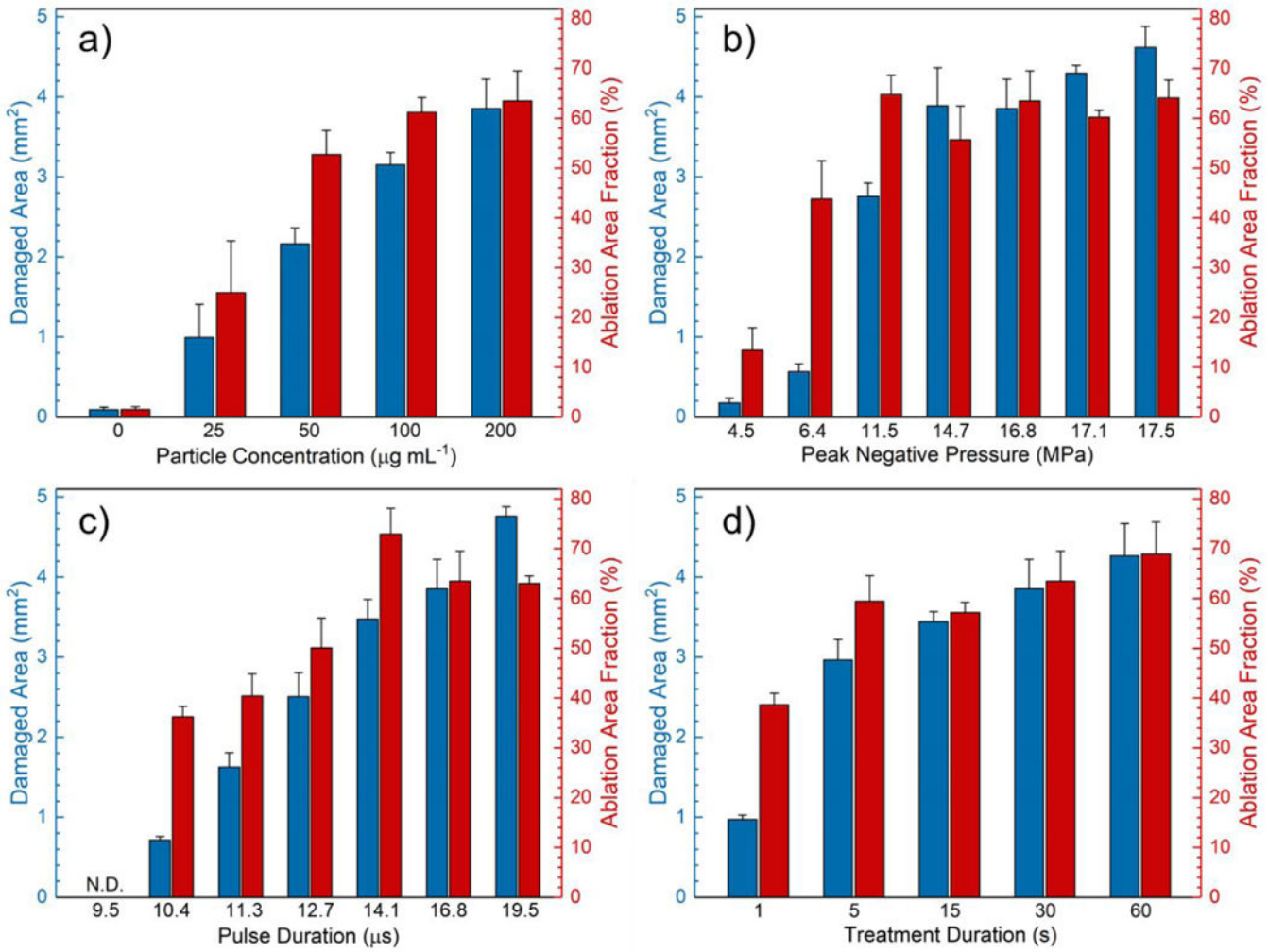

Figure 3.

Effects of HIFU parameters on the damaged area and ablation area fraction. a) Damaged area and ablation area fraction in the RBC phantoms containing PL-hMSN at different concentrations after HIFU treatment for 30 s at a pulse duration of 16.8 μs, a pulse repetition frequency of 10 Hz (duty cycle of 0.017%), and peak negative pressure of 16.8 MPa. b) Damaged area and ablation area fraction in the RBC phantoms containing PL-hMSN (200 μg mL^{-1}) after HIFU treatment at the different peak negative pressures for 30 s at a pulse duration of 16.8 μs and a pulse repetition frequency of 10 Hz (duty cycle of 0.017%). c) Damaged areas and ablation area fraction in the RBC phantoms containing PL-hMSN (200 μg mL^{-1}) after HIFU treatment at different pulse durations for 30 s at a peak negative pressure of 16.8 MPa and a pulse repetition frequency of 10 Hz. d) Damaged area and ablation area fraction in the RBC phantoms containing PL-hMSN (200 μg mL^{-1}) after HIFU treatment for different durations at a peak negative pressure of 16.8 MPa, a pulse duration of 16.8 μs, and a pulse repetition frequency of 10 Hz (duty cycle of 0.017%). Error bars = 1 SD, studies were run in triplicate.

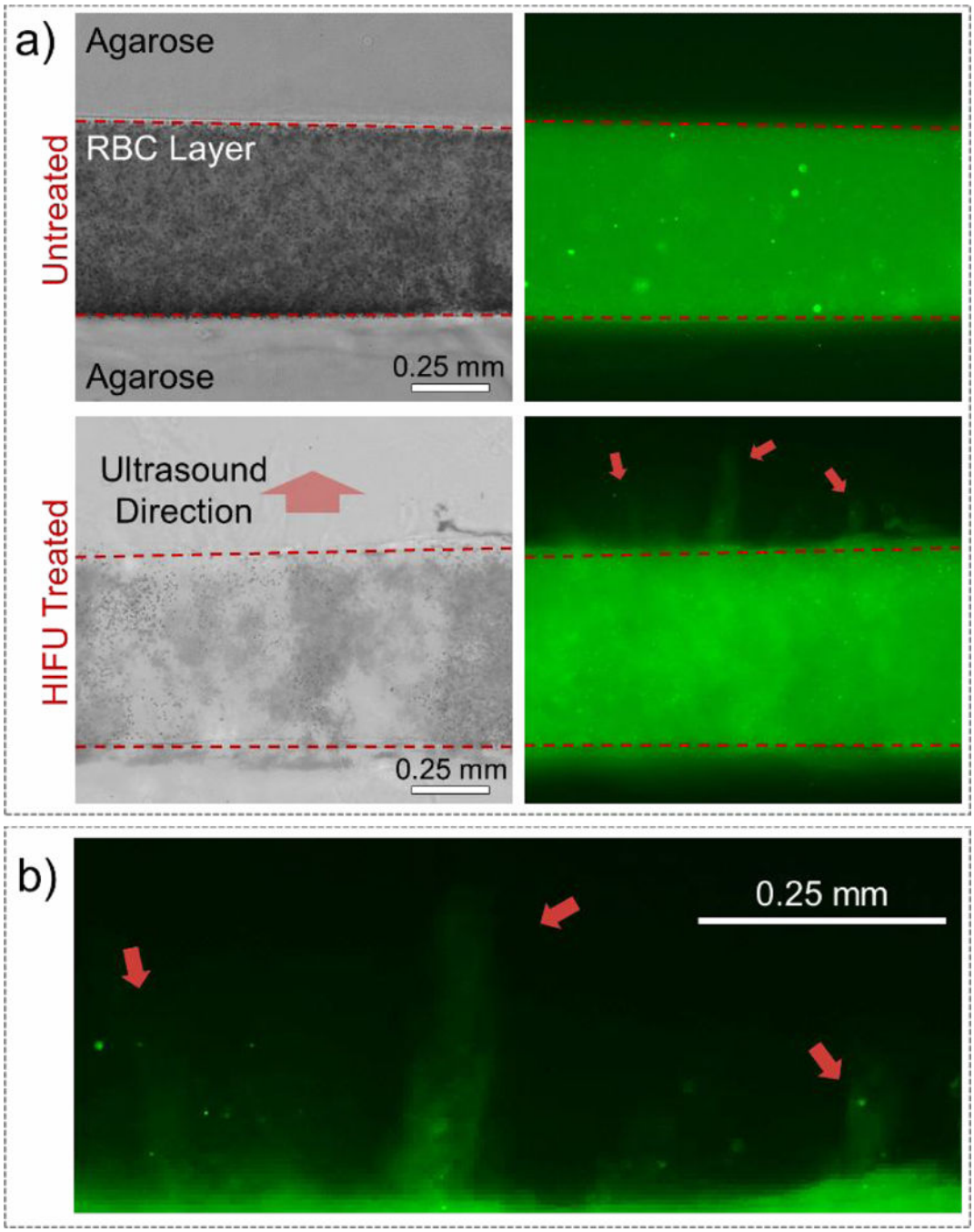

Figure 4.

a) Cross-sectional bright field (left) and fluorescence (right) images of the RBC phantoms containing PL-hMSN (200 μg mL^{-1}) before and after HIFU treatment for 30 s at a pulse duration of 16.8 μs, a pulse repetition frequency of 10 Hz (duty cycle of 0.017%), and peak negative pressure of 16.8 MPa. b) Close-up of the bottom right image in a), showing the PL-hMSN penetration into the agarose layer after HIFU treatment.

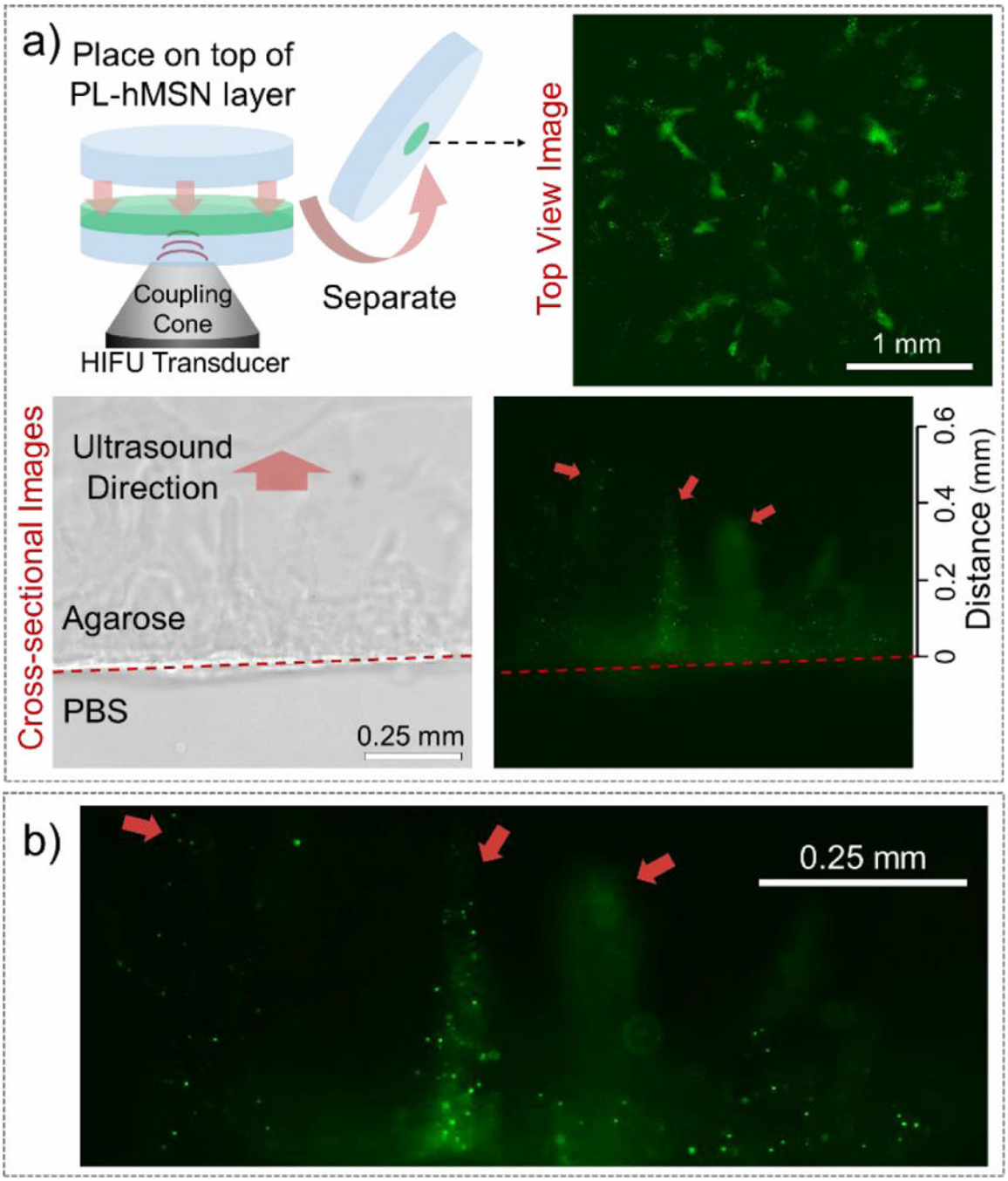

Figure 5.

a) (top left) Schematic showing the nanoparticle penetration to adjacent agarose gel experiments, where two gels (one double-layered with a thin layer containing PL-hMSN and a thicker agarose layer, and one pure agarose gel) placed together and treated with HIFU for 30 s at a pulse duration of 16.8 μs, a pulse repetition frequency of 10 Hz (duty cycle of 0.017%), and peak negative pressure of 16.8 MPa. Then, gels were separated, and PL-hMSN penetration into to the pure agarose gel was observed under the microscope from the top (top

right) and the cross-section (bottom). b) Close-up of the bottom right image in a), showing the PL-hMSN penetration into the agarose layer after HIFU treatment.

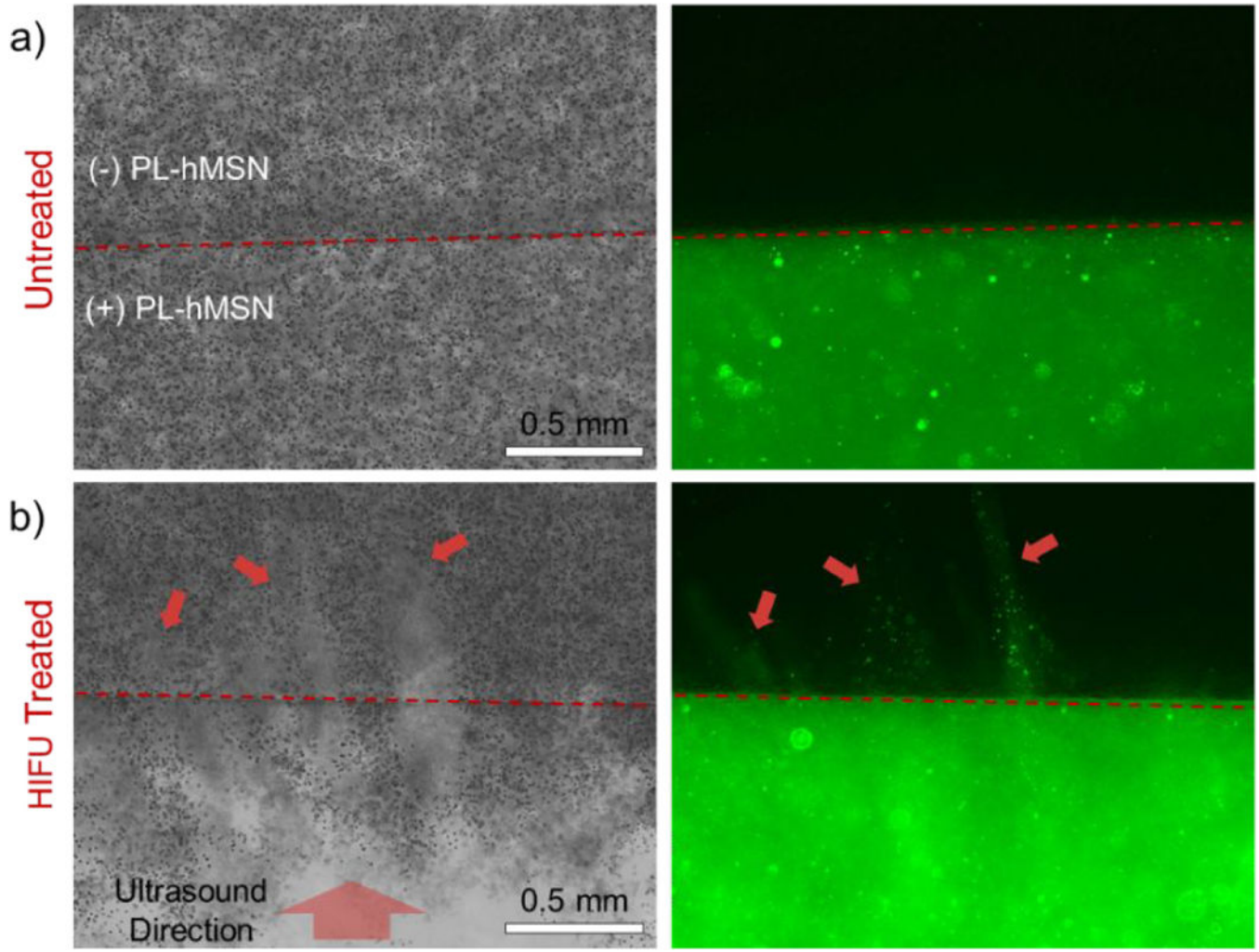

Figure 6.

Cross-sectional bright field (left) and fluorescence (right) images of the a) untreated and b) HIFU treated RBC phantoms containing PL-hMSN (200 μg mL^{-1}). HIFU treatment was performed for 30 s at a pulse duration of 16.8 μs, a pulse repetition frequency of 10 Hz (duty cycle of 0.017%), and peak negative pressure of 16.8 MPa. Red arrows highlight the damaged regions of the PL-hMSN-free layer and PL-hMSN penetration into this layer.

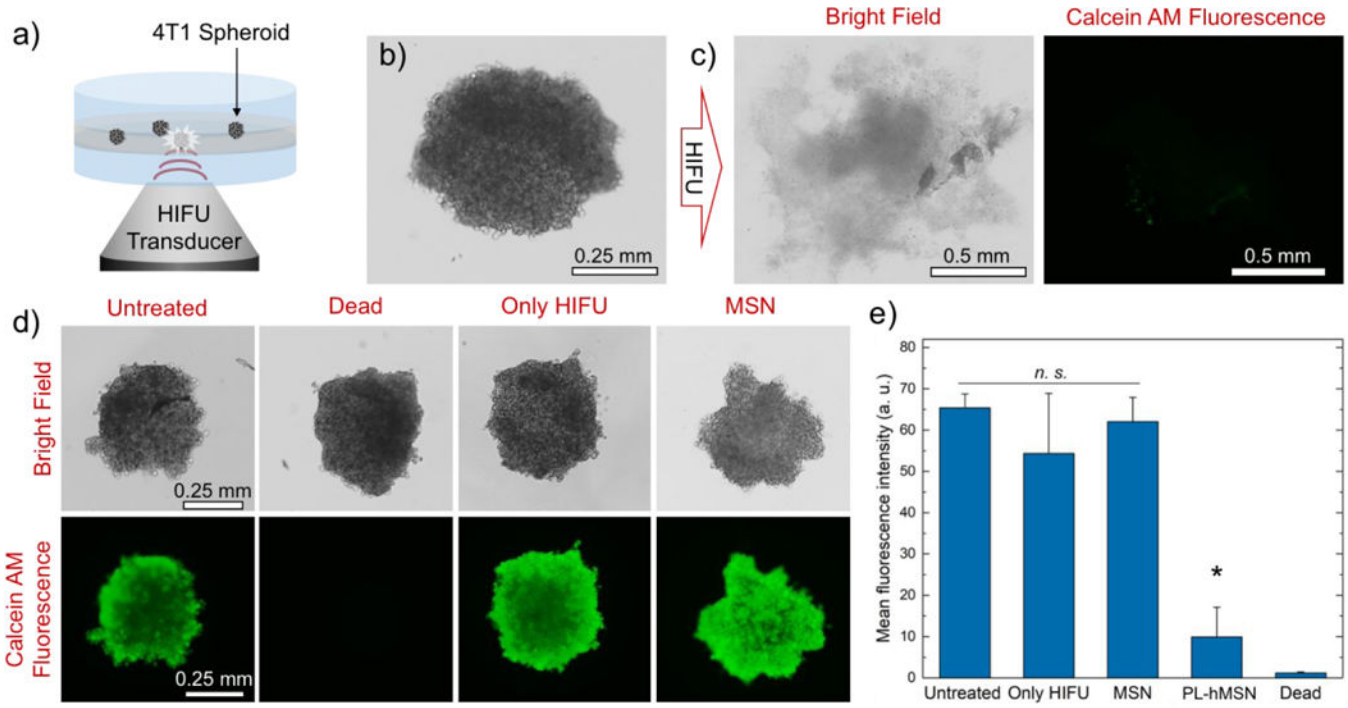

Figure 7.

a) Schematic representation of the spheroid phantom and its treatment with HIFU. b) Typical appearance of a 4T1 spheroid encapsulated in a phantom. c) Bright field and fluorescence images of the spheroid in b) after HIFU treatment for 30 s at a pulse duration of 16.8 μs, a pulse repetition frequency of 10 Hz (duty cycle of 0.017%), and peak negative pressure of 16.8 MPa in the presence of PL-hMSN (200 μg mL^{-1}). Spheroid was stained with Calcein AM for fluorescence imaging. d) Bright field and fluorescence images of Calcein AM stained spheroids, which were untreated or treated with HIFU in the presence of MSN (200 μg mL^{-1}) or the absence of any nanoparticles. e) Mean fluorescence intensity of the Calcein AM stained spheroids untreated or treated with HIFU in the presence of PL-hMSN or MSN (200 μg mL^{-1}) or the absence of any nanoparticles. Error bars = 1 SD. Studies were run at least in triplicate, and statistical significance (*) was determined using a Wilcoxon Rank Sum Test at $\alpha = 0.025$ for a one-tailed distribution relative to Untreated.